





Review

Main Results from the ISSI International Team “Characterization of 67P Cometary Activity”

Andrea Longobardo ^{1,*}, Minjae Kim ^{2,3}, Boris Pestoni ⁴, Mauro Ciarniello ¹ , Giovanna Rinaldi ¹, Stavro Ivanovski ⁵, Fabrizio Dirri ¹, Marco Fulle ⁵ , Vincenzo Della Corte ⁶, Alessandra Rotundi ^{1,7}  and Martin Rubin ⁴ 

- ¹ INAF-IAPS, Via Fosso del Cavaliere 100, 00133 Rome, Italy; mauro.ciarniello@inaf.it (M.C.); giovanna.rinaldi@inaf.it (G.R.); fabrizio.dirri@inaf.it (F.D.)
- ² Space Research Institute of the Austrian Academy of Sciences, Schmiedlstrasse 6, 8042 Graz, Austria; minjae.k.kim@warwick.ac.uk
- ³ Department of Physics, University of Warwick, Gibbet Hill Road, Coventry CV4 7AL, UK
- ⁴ Space Research & Planetary Sciences, Physics Institute, University of Bern, CH-3012 Bern, Switzerland; boris.pestoni@unibe.ch (B.P.); martin.rubin@unibe.ch (M.R.)
- ⁵ INAF-OATS, Via G.B. Tiepolo 11, 34143 Trieste, Italy; stavro.ivanovski@inaf.it (S.I.); marco.fulle@inaf.it (M.F.)
- ⁶ INAF-Osservatorio Astronomico di Capodimonte, Salita Moirariello 16, 80131 Napoli, Italy; vincenzo.dellacorte@inaf.it
- ⁷ DIST, Centro Direzionale Isola C4, Università di Napoli ‘Parthenope’, 80143 Naples, Italy
- * Correspondence: andrea.longobardo@inaf.it

Abstract: The ESA/Rosetta mission accompanied the Jupiter Family Comet 67P/Churyumov-Gerasimenko and provided a huge amount of data which are providing important results about cometary activity mechanisms. We summarize the results obtained within the ISSI International Team *Characterization of 67P cometary activity*, which studied dust and gas ejection in different stages of the comet’s orbit, by means of a data fusion between instruments onboard the Rosetta orbiter, i.e., the OSIRIS camera, the VIRTIS imaging spectrometer, the GIADA dust detector, the MIDAS atomic force microscope, the COSIMA dust mass spectrometer, and the ROSINA gas mass spectrometer, supported by numerical models and experimental work. The team reconstructed the motion of the dust particles ejected from the comet surface, finding a correlation between dust ejection and solar illumination as well as larger occurrence of fluffy (pristine) particles in less processed and more pebble-rich terrains. Dust activity is larger in ice-rich terrains, indicating that water sublimation is the dominant activity process during the perihelion phase. The comparison of dust fluxes of different particle size suggests a link between dust morphology and ejection speed, generation of micrometric dust from fragmentation of millimetric dust, and homogeneity of physical properties of compact dust particles across the 67P surface. The comparison of fluxes of refractory and ice particles suggests the occurrence of a small amount of ice in fluffy particles, which is released when they are fragmented. A new model of cometary activity has been finally developed, according to which the comet nucleus includes Water-Ice-Enriched Blocks (WEBs), that, when exposed by CO₂ activity, are the main sources of water sublimation and dust ejection.

Keywords: comet: Churyumov-Gerasimenko; dust; planetary surfaces; planetary dust



Citation: Longobardo, A.; Kim, M.; Pestoni, B.; Ciarniello, M.; Rinaldi, G.; Ivanovski, S.; Dirri, F.; Fulle, M.; Della Corte, V.; Rotundi, A.; et al. Main Results from the ISSI International Team “Characterization of 67P Cometary Activity”. *Universe* **2023**, *9*, 446. <https://doi.org/10.3390/universe9100446>

Academic Editor: Lorenzo Iorio

Received: 18 September 2023

Revised: 4 October 2023

Accepted: 8 October 2023

Published: 11 October 2023



Copyright: © 2023 by the authors. Licensee MDPI, Basel, Switzerland. This article is an open access article distributed under the terms and conditions of the Creative Commons Attribution (CC BY) license (<https://creativecommons.org/licenses/by/4.0/>).

1. Introduction

The ESA’s Rosetta mission orbited the 67P/Churyumov-Gerasimenko comet from 2014 to 2016 and escorted it from pre- to post-perihelion. During pre-perihelion, the comet was not very active and was mainly affected by previous perihelion passages and processes far from the sun (e.g., cosmic rays hitting the nucleus, fallout self-cleaning). Perihelion (13 August 2015) was the peak of activity due to water ice sublimation and the consequent dust and gas emissions. After perihelion, the comet was rejuvenated from the perihelion activity.

The Rosetta mission gave a unique opportunity to study for a long time a Jupiter Family Comet, giving clues about the formation, evolution, and activity of these bodies, which are among the most primitive in the Solar System and therefore related to its formation and early stages of its evolution.

The ISSI (International Space Science Institute) International Team “Characterization of 67P cometary activity” was aimed at exploiting and combining data from several instruments onboard the Rosetta spacecraft to understand issues related to comet activity by means of data fusion, comparison with models, and laboratory experiments. In 2019, ISSI selected this proposal, and several studies were conducted. This paper summarizes the main results obtained during this project, referring to previously published papers for details.

Section 2 describes the state of the art before the start of the project, while Section 3 is devoted to the project goals. Studies developed during the ISSI International Team project and published, as well as studies in progress, are shown in Section 4, while the main results are summarized in Section 5.

2. State of the Art

The project merged data from different instruments onboard the Rosetta spacecraft, i.e., the VIRTIS (Visible and Infrared Thermal Imaging Spectrometer [1] and Alice [2] spectrometers, the OSIRIS (Optical, Spectroscopic and Infrared Remote Imaging System) camera suite [3], the GIADA (Grain Impact Analyser and Dust Accumulator) dust detectors [4], the MIDAS (Micro-Imaging Dust Analysis System) atomic force microscope [5], and the COSIMA (Cometary Secondary Ion Mass Analyser) [6] and ROSINA (Rosetta Orbiter Spectrometer for Ion and Neutral Analysis) [7] dust and gas mass spectrometers, respectively. In this section, we summarize the main results obtained by these instruments before the start of the project.

OSIRIS mapped the entire comet surface [8,9]. The comet is bilobated and composed of four macro-regions, i.e., head, neck, body, and bottom, which in turn include rougher/older and smoother/younger terrains. The most active periods and regions were identified by surface changes [10] and brightness variations in the coma [11].

VIRTIS spectra identified the ubiquitous presence of organics [12,13] and ammoniated salts [14] on the comet surface from the reflectance absorption features centered at 3.2 μm . Nevertheless, temporary exposure of water ice was detected by shortward shift of this band, by flattening of the visible and infrared slopes [15], and by appearance of 1.5 and 2.0 μm bands [16]. The abundance of water ice on the comet surface shows both a diurnal [17] and a seasonal [18] variation, with water ice patches’ presence increasing as the comet approaches perihelion [19,20]. The VIRTIS observations of the coma found a correlation between water vapor and dust distribution in the coma, indicating that water vapor is the main gas driving the dust emission [21].

Alice characterized the gas counterpart of outbursts (i.e., sudden ejection of gas and dust) as H_2O , CO_2 , CO , and O_2 . H_2O , CO_2 , CO , and O_2 were all indirectly observed in Alice UV spectra via emission from the daughter products H, C, and O as the first three members of the H I Lyman series, O I multiplets at 1152, 1304, and 1356 Å, and weak multiplets of C I at 1561 and 1657 Å [22].

Dust detectors identified two populations of dust: fluffy and compact particles. Fluffy particles have a porosity larger than 95% and are particularly interesting because they are the most primitive and linked to presolar grains. They can be fragmented from spacecraft electrostatic potential; therefore, in the following, we use the terms “fluffy parent particles” to identify particles as ejected from the surface and “fluffy fragments” to identify particles generated from the fragmentation of fluffy parent particles. Compact particles include solid and porous particles, i.e., all the particles with a porosity lower than 95%.

The GIADA dust detector was composed of three subsystems, i.e., the Grain Detection System (GDS), which measured the speed of larger dust particles (e.g., mm-sized, mainly fluffy particles), the Impact Sensor (IS), which measured the momentum of compact

particles (e.g., tens to hundreds of microns), and then the Microbalance System (MBS), which measured the cumulative mass of lighter (e.g., ng to μg) dust particles. The spatial distributions of fluffy and compact particles in the coma are not correlated [23].

MIDAS collected and studied the 3D structure of μm -sized particles, which were found to be agglomerated [24]. MIDAS detected dust in four specific periods, three related to the pre-perihelion stage and one to a post-perihelion outburst (i.e., 21 February 2016). Except for one case, MIDAS detected only compact particles, since it was designed to detect smaller particles.

The dust particles detected by COSIMA are fragments tens of microns in size and belong to the compact particle population [25]. Most of the particles were fragmented in the instrument funnel, but [25] developed an algorithm to retrieve the number of parent particles hitting the instrument. The suggested composition of particles is about 50% organic matter [26] and about 50% other anhydrous mineral phases, with the occurrence of Calcium Aluminium Inclusions (CAIs) [27].

ROSINA monitored the gas densities at the location of Rosetta. From these measurements, the gas activity, i.e., production rate of different volatile species during the mission, was derived [28–30]. A link between organics detected in the coma and those detected on the surface by the Philae lander was found [31].

3. Project Goals

The activity of this ISSI International Team was divided into two Work Packages:

- *WP1: Traceback.* The objective of this WP was to trace the coma dust motion down to the nucleus surface. To this end, an algorithm was developed [32], based on assumptions given by dust dynamical models [33]. The application of this algorithm allowed for associating each dust particle detected in the coma with its source terrain and studying the relation between dust porosity/morphology and surface geomorphology, giving hints about comet formation mechanisms.
- *WP2: Data Fusion.* This WP related WP1 outcomes with geometric information and with data provided by different instruments onboard Rosetta. This allowed studying the following relationships: activity vs. illumination conditions, dust emission vs. surface composition, dust morphology vs. dynamics, and dust vs. ice ejection. Each of these studies provided a new piece of the puzzle to understand comet formation and activity. Taking inputs from these studies, a water ice activity model was developed.

4. Results

4.1. Traceback

GIADA Data Analysis

For details of this work, refer to [32,34].

The GIADA's GDS and IS datasets included three types of detections: (a) GDS-only detections, in turn divided in (a1) dust showers, i.e., ensembles of particles detected within a time interval lower than 1 s between two successive detections, and (a2) GDS single detections; (b) IS-only detections; (c) GDS + IS detections, i.e., particles detected by both subsystems. GDS+IS detections were used to obtain a relation between velocity and momentum [23], which was then used to retrieve the speed of IS-only detections. According to GIADA calibration activity and dust modelling [35], GDS + IS, IS-only detections, and GDS-only single detections were associated with compact particles, and GDS-only dust showers with fluffy particles. Because dust showers are due to the fragmentation of a single fluffy particle due to the electrostatic potential of Rosetta, we associated each dust shower with a single fluffy particle (i.e., the parent particle); its speed was retrieved as the median of the most populated bin of the shower's speed distribution (the bin size is 5 m/s).

To trace back the dust particles' motion, we made the following assumptions, based on dust dynamical models: (a) radial motion; (b) constant acceleration up to 11 km height and constant speed above that height. According to numerical models (e.g., [33,36]), these assumptions are valid for low heights (a threshold of about 70 km was determined

a posteriori), because at higher altitudes, dust particles tend to deviate from the radial trajectory, due to the increasing effect of solar radiation pressure.

The traceback algorithm was firstly applied to the inbound arc from September 2014 to January 2015 (spacecraft altitude lower than 40 km). Each particle was associated with the source region, based on the geomorphological classification by [8,9]. Then, the ejection rate (per surface unit) of compact and fluffy particles was retrieved for each geomorphological region on the comet. We concluded that emissions of fluffy and compact particles are correlated at the surface, although their spatial distributions in the coma are not (Figure 1). This means that fluffy and compact particles are ejected together and then spread in the coma due to their different speed. In addition, a correlation between dust ejection rate and solar illumination was found (Figure 2), indicating that the latter is the main, if not the only driver, of cometary dust activity.

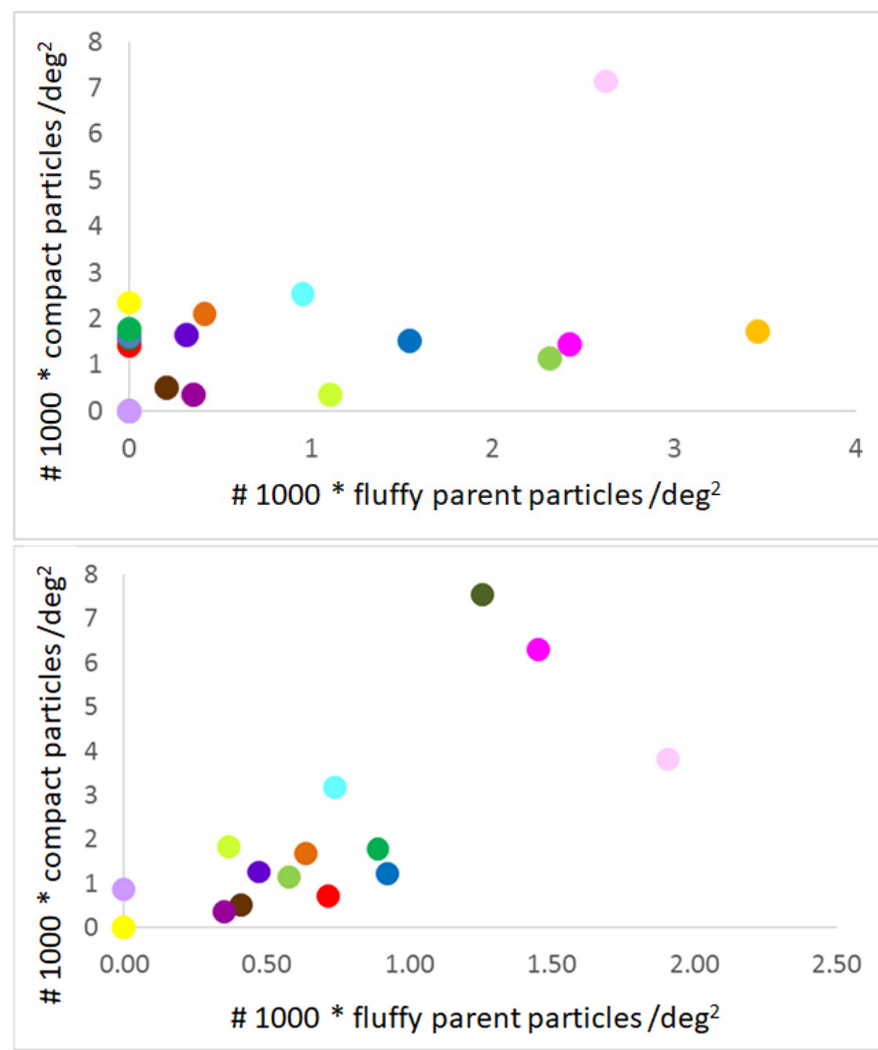


Figure 1. Relation between compact particles and fluffy parent particles before (**top**) and after (**bottom**) the application of the traceback algorithm (the number of compact and fluffy parent particles has been multiplied by 1000 for a better representation). Each dot corresponds to a different geomorphological region (for interpretation of colors, refer to [32]). Before the application of the traceback (**top**), a dust particle has been assigned to a specific region by projecting the spacecraft position on the surface. No correlation is found in the coma (**top**), while the two dust populations are correlated on the nucleus surface (**bottom**).

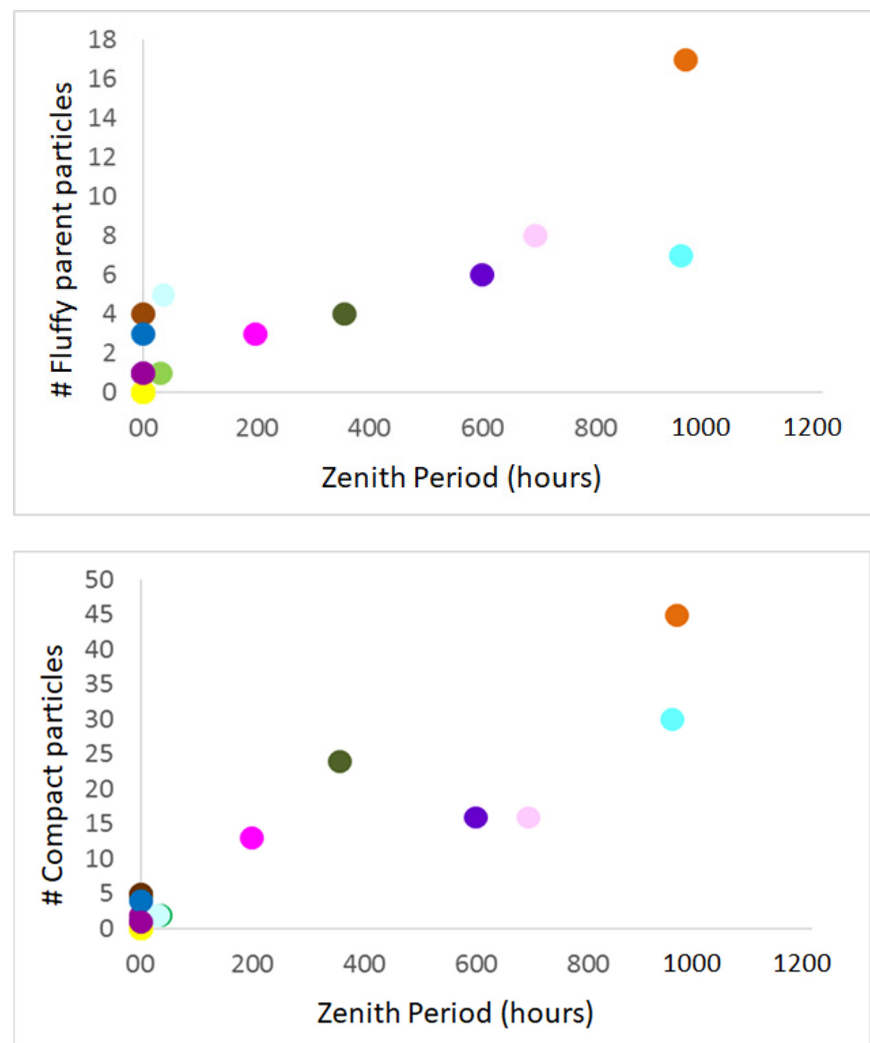


Figure 2. Number of parent fluffy (**top**) and compact (**bottom**) dust particles as a function of the numbers of hours spent under normal solar illumination. Each dot corresponds to a different geomorphological region (for interpretation of colors, refer to [32]). Before the application of the traceback (**top**), a dust particle has been assigned to a specific region by projecting the spacecraft position on the surface. A correlation between dust ejection and solar illumination is found.

This procedure was then extended to other mission periods, giving similar results in periods where the spacecraft altitude was lower than 70 km (January–March 2015 and February–September 2016), while from April 2015 to January 2016 (period including the comet perihelion), no correlation was found at all, due to the large spacecraft altitude (i.e., >100 km) and consequent unreliability of the assumptions of our traceback procedure.

Then we studied the fraction of fluffy and compact particles ejected from rough and smooth terrains, in order to obtain a relation between dust porosity and surface geomorphology. The discrimination between rough and smooth regions was provided by the geomorphological classification by [8,9]. We focused on orbital distances lower than 3.0 au, because for larger heliocentric distances, the ejection is dominated by dust particles previously ejected and then fallen back, rather than by direct dust emission [37,38]. We found that the abundance of fluffy particles in rough terrains is 23 ± 9 per cent larger. According to comet formation models [35,39], fluffy particles were embedded between cm-sized pebbles, responsible for terrain roughness, and the volume available for fluffy particles is 37 ± 5 per cent larger in rough terrains, in agreement with our estimate.

4.2. Data Fusion

4.2.1. GIADA vs. VIRTIS

For details of this work, refer to [32].

GIADA and VIRTIS data were combined to relate the dust ejection rate, as measured by the dust detector, with surface compositional changes, as revealed by the imaging spectrometer. The fluffy and compact dust ejection rate per surface unit was retrieved in the WP1 activity.

We focused on the spectral parameters indicating water ice exposure, i.e., the center of the $3.2\ \mu\text{m}$ absorption band and the infrared spectral slope (i.e., between 1.1 and $2.0\ \mu\text{m}$); both parameters decrease with increasing water ice abundance. This behavior is observed in the pre-perihelion stage at larger surface temperature, when activity increases and consequently underlying water ice is exposed [20]. The result was confirmed by relating the compact and fluffy dust ejection rate (GIADA indicator) of each geomorphological region with their variation in band center and spectral slope (VIRTIS indicator). The correlation between the GIADA and VIRTIS indicators (Figure 3) shows that dust activity is stronger in ice-rich terrains.

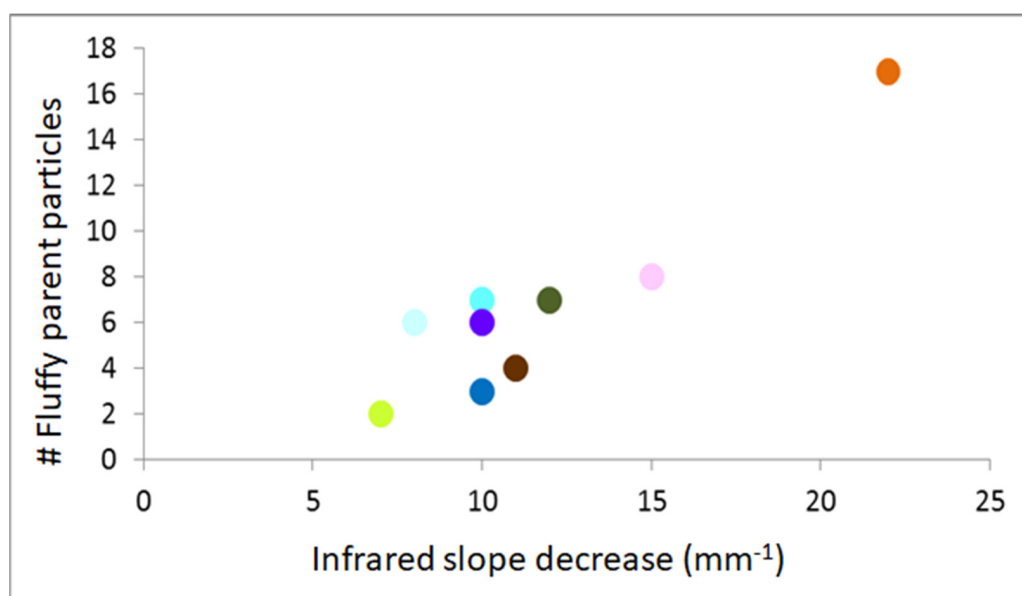


Figure 3. Number of fluffy parent particles ejected from each region as a function of the variation in the infrared slope. Each dot corresponds to a different geomorphological region (for interpretation of colors, refer to [20]). A larger slope variation indicates a higher flattening. The correlation between the two indicators reveals that higher dust ejection is related to larger water ice exposure, i.e., ice-rich terrains are more active. The same behavior is observed by considering other GIADA (i.e., ejection rate of compact particles) and VIRTIS (i.e., $3.2\ \mu\text{m}$ band center shift) indicators.

4.2.2. MIDAS Data Analysis and MIDAS vs. GIADA

For details of this work, refer to [32,40,41].

A new version of the catalogue of the dust particles detected by MIDAS was obtained, by adding particles, correcting errors, and adding shape descriptors with respect to the version previously available on the ESA PSA (Planetary Science Archive).

Two radius estimates of each particle were retrieved. The average radius based on the 2D projection is $0.9 \pm 0.8\ \mu\text{m}$, while that obtained from the volume distribution, i.e., taking into account the 2D projection and the particle height, is $0.56 \pm 0.45\ \mu\text{m}$; this indicates that particles are flattened from the impact on the MIDAS targets. The size distribution is shown in Figure 4; its index spans from -1.88 ± 0.04 (volume-based) to -1.67 ± 0.11 (projection-based).

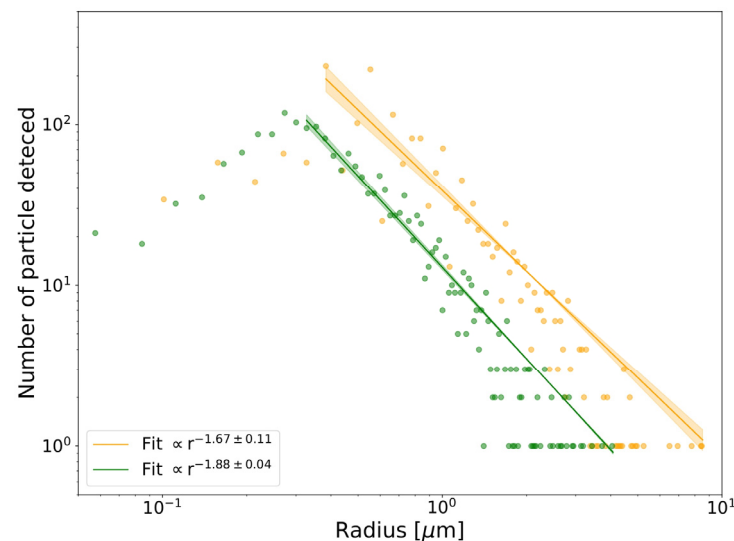


Figure 4. MIDAS particle size distributions with radii based on the 2D projection combined with a power law $a \cdot r^b$ fit with an index b of $\sim -1.67 \pm 0.11$ (yellow line) and the one derived from volume with an index b of $\sim -1.88 \pm 0.04$ (green line).

The analysis of MIDAS dust particles aimed at comprehending the extent of dust alteration and identifying the structural properties that remained unchanged during the collection process.

Various independent 2D and 3D shape descriptors and morphological parameters were employed, including aspect ratio (Height/ $\sqrt{\text{Area}}$; [42]), elongation [43], circularity (Area/perimeter; [44]), and convexity (Area/convex Area; [44]), alongside particle surface and volume distributions. Furthermore, qualitative comparisons were also carried out between the morphologies of MIDAS deposits and those observed by COSIMA and previous laboratory studies.

The mean aspect ratio of MIDAS particles is 0.53 ± 0.40 , indicating particle flattening during collection. Furthermore, the mean elongation is 3.93 ± 2.31 , revealing substantial deviation from a spherical shape. Similarly, circularities exhibit a mean value of 0.58 ± 0.19 , signifying departure from circularity. Additionally, the convexity value of MIDAS particles stands at 0.47 ± 0.19 , meaning that most of the convex hull area of MIDAS particles is occupied by their perimeter concavities.

No discernible correlations were found between shape descriptors and properties related to the target, implying that variations in dust activities and cometary source regions, as well as differing collection velocities, do not significantly impact particle structural alterations at the micrometer scale. Notably, the aspect ratio distributions of particles of different cluster morphologies, such as MIDAS single, footprints, and pyramid clusters [41], show homogeneity in properties. Aspect ratio distributions remain strikingly consistent across various cluster types, suggesting similarities in shape and composition among their sub-units. Finally, MIDAS clusters and their aspect ratio distribution show both similarities and differences to those found by COSIMA. Based on the findings and experimental results from [45,46], the MIDAS single cluster seems to contain the least altered particles.

Based on the shape descriptors of MIDAS particles and comparative findings, a final pristineness score by weighting and knowledge about seemingly pristine morphologies is calculated. Among 1082 MIDAS particles, only 1 particle achieved a highly pristine rating, while 18 particles were categorized as moderately pristine. In contrast, 222, 354, and 474 particles were, respectively, classified as possibly altered, altered, and severely altered. This underscores the inevitability of dust alteration, even at the relatively slow collection speeds employed by the Rosetta spacecraft.

The particle catalog [40] and shape descriptor [41] will serve as references for future scientific projects such as the development of more realistic analogue materials, and the design of dust particles in simulations for comets and early solar system studies.

Since particles collected by MIDAS consist of fragments created from the parent particles' impact on the instrument funnel and/or target, two methods to obtain the number of parent particles hitting the MIDAS targets were applied to compare dust fluxes measured by several instruments onboard Rosetta. One method is empirical and assumes that particles clustered in the same target area within two times the particle size and detected in the same exposition period belong to the same parent particle. Another method is the mean shift algorithm, which assigns each particle to a cluster (i.e., to a parent particle) by shifting points towards the highest density of data points (details in [40]).

For each MIDAS' exposition period, we retrieved the dust flux measured by MIDAS and GIADA as well as the average dust speed and the dust surface source obtained from GIADA data and the traceback algorithm described in Section 4.1.

While both MIDAS and GIADA measured the largest dust flux during the 19/02/16 outburst, the ratio between the two dust fluxes is constant over time within errors, regardless of the clustering method used on MIDAS data. The same result is obtained by considering the dust flux measured by COSIMA in the same periods [25]. Because MIDAS and GIADA detected micron-sized particle and particles hundreds of microns to millimeters in size, respectively, and activity models predict that only the latter can be lifted by water sublimation [47], we inferred that the small particles detected by MIDAS are fragments of larger particles, like those detected by GIADA. This occurs even during the February 2016 outburst, when in principle an ejection of particles microns and hundreds of nanometers in size could occur, as observed for other outbursts by [48]. The obtained result suggested that such small particles were not ejected during the 21/02/16 outburst, different from what was observed in other outbursts.

The four MIDAS targets collected particles coming from terrains having different roughness. Nevertheless, no variation in dust morphology indicators was observed among the targets, i.e., average size, dust size distribution index, flatness, elongation (for details about these values, refer to [40,49]). This means that properties of compact dust particles are similar across the comet's surface.

Otherwise, a correlation between dust physical properties and speed is found. Specifically, when the speed is higher, smaller and lighter dust particles are able to reach the MIDAS detectors. Moreover, faster particles are more flattened from the impact on the target.

4.2.3. ROSINA Data Analysis and ROSINA vs. GIADA

For details of this work, refer to [50–52].

The ROSINA-COPS pressure/density sensor is composed of two density gauges; the ram gauge measured the ram pressure/density, while the nude gauge measured the total neutral density. During the Rosetta mission, icy particles were detected in the two COPS gauges and the results were compared with GIADA in order to study the sublimation of icy grains near Rosetta and the relation between the different particle fluxes.

The COPS ram gauge detected 73 icy particles as density peaks that were ascribed to sublimation of their volatile content. From the temporal decay of the signal, it was concluded that species of different volatility were observed, e.g., from water to organics. However, since COPS could only measure density and not composition, we refer to, e.g., [31], who measured the composition of impacting grains in the ROSINA mass spectrometer during a dust outburst. The average radius of an equivalent sphere of volatiles of these icy particles has been estimated to be of the order of hundreds of nanometers based on the integrated signal inside the COPS ram gauge.

Due to its better signal-to-noise ratio, larger field of view, and longer operation time, the nude gauge detected about 67,000 icy particles. This number was obtained after removal of artifacts, i.e., signals produced by thruster operations, spacecraft background, and noise due to elevated fluxes of energetic electrons. The retrieved nude gauge detection

rate is anticorrelated with the comet's heliocentric distance and is correlated with its gas production rate (estimated with the Haser model, [53]), with the water production rate [54], and with the coma's dust brightness. These trends link icy particle detection to cometary activity. By assuming icy particles to be pure water ice spheres, a size range between 60 and 390 nm and a dust size distribution index of -4.79 ± 0.26 were found.

GIADA-GDS, GIADA-IS, GIADA-MBS, and ROSINA-COPS data were combined to study the relation between the ejection of dust (fluffy parent particles, fluffy fragments, compact particles, and nanogram dust) and icy particles. The only correlation found was between fluffy parent and icy particles (Figure 5), with a Pearson coefficient (i.e., the ratio between the covariance and the product of the two standard deviations) of 0.55, indicating a moderate correlation. We inferred that icy particles are released from the fragmentation of fluffy particles. From the smallest subunit size observed on dust particles (i.e., 52–183 nm, [55]) and from the retrieved volume of each icy particle, we obtained that each COPS detection sensed between 1 and 15 icy volatile subunits. This means that the icy component of dust particles is very small and that parent fluffy particles are almost totally dehydrated, probably because of their fractal structure, which exposes them to more sunlight on their journey to the spacecraft (several hours to days).

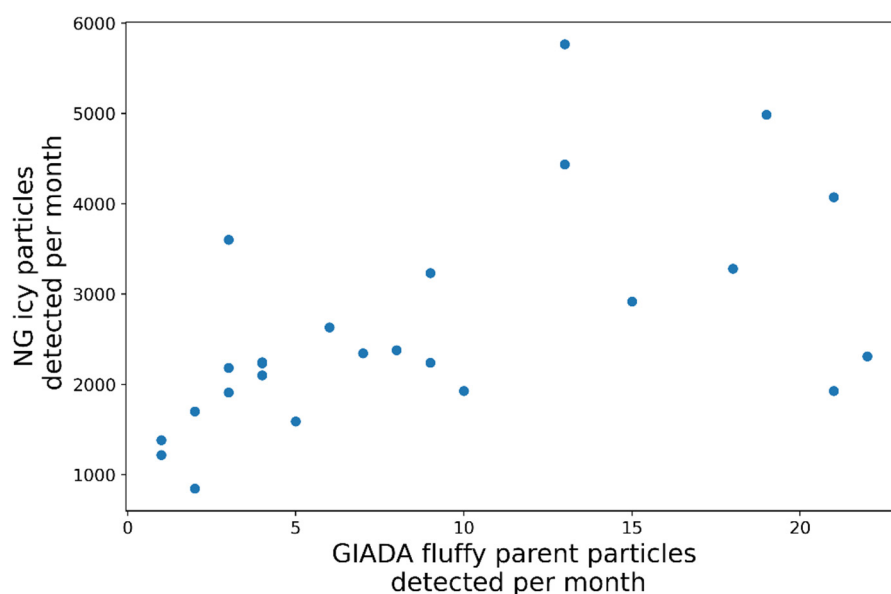


Figure 5. Relation between icy particles detected by the ROSINA-COPS's nude gauge (NG) and the fluffy parent particles detected by GIADA-GDS. Each dot refers to a different month of the Rosetta mission. A moderate correlation arises.

4.2.4. Alice vs. VIRTIS

For details of this work, refer to [56,57].

Alice and VIRTIS data were combined to analyze the dust and gas component of outbursts observed on 67P from the ultraviolet to infrared wavelengths. Cometary outbursts offer a valuable window into the composition of comet nuclei with their forceful ejection of dust and gas, which reveals the interior components of the comet. Understanding how different types of outbursts influence the observed dust properties and volatile abundances is necessary to interpret what signatures can be attributed to primordial composition and what features are the result of processing.

Alice outburst spectra show the transient events characterized by a variation in $\text{CO}_2/\text{H}_2\text{O}$ and $\text{O}_2/\text{H}_2\text{O}$ ratio, as determined from spectral modelling and different observed O I 1356/O I 1304 Å ratio (i.e., ratio between emission at the two wavelengths). In cases where dissociative electron impact excitation on O_2 or CO_2 is dominant, we would expect an O I 1356/O I 1304 Å ratio greater than 1, while if dissociative electron impact

occurs on H₂O, this value would be less than 1 [22,56]. Some outbursts contained more CO₂ and O₂, while other were relatively richer in H₂O. Elevated CO₂ content could indicate a more pristine surface origin (i.e., fracture deepening) and the high activity can last for hours before returning to a typical dust environment.

VIRTIS detected and characterized the dust properties of the outburst in terms of light curve, color, and dust mass loss in the VIS and IR wavelength range. The VIRTIS observations show two kinds of outbursts. The first type is characterized by strong color gradient values in the dust continuum with respect to the surrounding coma and the second type does not show color difference.

The outburst color sequence in the VIS and IR shows a color gradient pattern which seems correlated to the intensity of the dust radiance within the outburst. The first type of outburst shows a VIS color behavior reaching the bluer values of $6.0 \pm 1.4\%/100\text{ nm}$ and returning to the pre-outburst value of about $14\%/100\text{ nm}$. The IR continuum emission is also characterized by high color temperatures of about 600 K and a bolometric albedo of 0.6 [48,56,58]. Color temperatures of 600 K thus reveal the presence of very small grains (less than 100 nm) in the outburst material. The bright grains in the ejecta could be silicate grains, implying the thermal degradation of the carbonaceous material, or icy grains. The rapid increase in radiance at the start of an outburst event is due to the release of small and bright silicate or icy particles with a high geometric albedo.

For the second type of outburst, we found no clear evidence of different reddening values in the dust continuum with respect to the surrounding coma. The reason is probably that this is a faint outburst and the signal from the background coma dominates, so the color of the outburst is not measurable. The VIS dust color is around $13.1\%/100\text{ nm}$ [48,56,58].

The outburst observations show that mixed gas and dust outbursts can exhibit different spectral signatures representative of their initiating mechanisms, with outbursts showing indicators of a cliff collapse origin or showing fresh volatiles being exposed via a deepening fracture. Preliminary results show that some cometary activity observed after outbursts has a moderate CO₂/H₂O ratio, evidence that CO₂ may have initiated the outburst and exposed new volatile-rich material. This analysis opens up the possibility of remote spectral classification of cometary activity with future work.

4.2.5. Cometary Activity Model

For details of this work, refer to [59].

Basing on the results provided by the Rosetta mission, including those obtained during this project, a model was developed to link the water activity mechanisms at the microscopic (sub-cm) scale with the seasonal evolution and the comet surface properties at the macroscopic (meter) scale.

According to [47], water ice activity in a pebble-made nucleus occurs when the dust erosion rate exceeds the dehydration rate. For 67P's gas emission rate [47] and nucleus density (538 kg/m^3 , [60]), this condition can be sustained at perihelic insolation conditions when the refractory-to-ice ratio is lower than 5. The spectral slope measured by VIRTIS shows a seasonal variation, being bluer at perihelion and redder with increasing heliocentric distance [18,59]; this indicates increasing water ice exposure (due to surface erosion from cometary activity) with approaching perihelion and successive dehydration or infall of dehydrated dust at larger heliocentric distances. Water ice exposure is not uniform across the surface but occurs mainly in a finite number of "blue patches". Modelling the spectral slope's temporal variation leads to the conclusion that the areal fraction of blue patches exposed at perihelion is less than 6%, according to activity model predictions [47].

These results suggest that the nucleus is mostly dehydrated but includes some Water-Ice-Enriched Blocks (WEBs), uniformly distributed across the nucleus, with a water ice abundance of about 50%. WEBs are exposed as blue patches by CO₂ activity, which is the activity process ejecting dm-sized chunks. Water-driven activity is enabled from blue patches, causes the ejection of small-sized dust (from microns to millimeters, depending on the surface temperature, [47]), and increases with increasing surface temperature. Once

exposed, WEBs are eroded by water-driven dust ejection. After perihelion, the surface fraction of blue patches decreases with the decay of CO₂ activity (and WEB exposure) and because dehydrated dust falls back and covers the surface.

From the estimated areal fraction of blue patches and assuming that CO₂ activity leads to chunk ejection [47], the WEBs' size is constrained in the 0.5–1 m range, in agreement with CONSERT radar and OSIRIS camera measurements [61,62].

The comet structure derived from this model is consistent with protoplanetary disk observations [63], where ice-rich and ice-poor dust grains are two separate populations; in these regions, WEBs can be formed as aggregates of water-ice-rich dust and then be incorporated within comets.

4.2.6. Modelling Dust Particles' Rotational Motion

For details of this work, refer to [64].

Based on the modelling efforts in recent years, the idea of developing a model that can simulate any kind of shape of different particles has evolved and consequently been extended to a universal approach that can be applied to compact and fluffy particles. Using a set of universal, dimensionless parameters characterizing the dust motion in the inner cometary coma, scaling laws of rotational motion applicable for any shape of particles were derived. The scaled values are compared with numerically computed ones by [33,65]. The parameter Iv characterizes the efficiency of entrainment of the particle within the gas flow (i.e., the ability of a dust particle to adjust to the gas velocity) and Fu characterizes the efficiency of gravitational attraction; their definition is given in Equations (15) and (16) in [33], respectively. For a given gas flow field, if two dust particles have the same Iv and Fu parameters (see [36,66] for details), their translational motion is similar. If, furthermore, they have the same R_n/a_d , where R_n is the radius of the nucleus and a_d is the size of the particle, then their rotational motion is similar as well. The derived scaling laws achieve precision in the scaled dust velocity and rotation frequency of more than 60–70% for compact spheroids and more than 95% for the velocity of prolate spheroids. These scaling laws can overcome sufficiently enough the bias that the sphericity can introduce in the simulations of realistic non-spherical dust grains, as observed by Rosetta OSIRIS [35] and MIDAS [40] instruments.

4.2.7. Experimental Work

The goal of this work is to simulate the photometric behavior of fluffy and compact dust particles and compare it to that observed on 67P's rough and smooth terrains [20].

To simulate fluffy and compact particles, different terrestrial minerals were selected and analyzed. Graphite (size < 300 µm) was used to assess the procedure and calibrate the signal spectrometer. Kaolinite mineral spontaneously tends to be fluffy, so coarse kaolinite was used to simulate fluffy dust and pressed kaolinite to simulate compact particles. Different grain size intervals were considered (i.e., 50–100 µm, 100–250 µm, 250–500 µm). A commercial spectrometer, i.e., Bruker Vertex 80 (spectral range: 0.6–1.2 µm, spectral resolution: 4 cm^{−1}), was used to study photometric behavior at phase angles of 30° (incidence 15°, emission 15°) and 60° (incidence 30°, emission 30°).

Preliminary results show the absence of a clear photometric trend between 30° and 60° phases of both coarse and pressed kaolinite, regardless of grain size. Reflectance variations are within 10%.

Experimental activity is still ongoing and new analogues are going to be selected, because kaolinite is too bright (i.e., reflectance of 0.9) and therefore is too affected by multiple scattering to study the photometric properties of 67P/Churyumov-Gerasimenko's dust.

5. Conclusions

The ISSI International Team *Characterization of 67P cometary activity* went into detail on the dust ejection mechanisms at play in comet 67P/Churyumov-Gerasimenko, and their relations with gas ejection and surface properties. The main results obtained throughout the project are the following:

- Fluffy and compact dust particles are ejected together from the mostly illuminated comet surface regions, then they are spread in the coma due to their different speeds.
- Dust ejection is higher in ice-rich terrains, as demonstrated by the correlation between dust ejection rate and spectral indicators of water ice exposure.
- Fluffy particles are more abundant in rough terrains, consistent with the theoretical model of incorporation within voids between pebbles when the comet formed.
- Compact dust's physical properties (e.g., size, flatness) are similar everywhere on the surface.
- Small dust particles in the coma (i.e., micron- and nm-sized) are mainly produced from the fragmentation of larger particles, directly ejected by water ice sublimation. During outbursts, dust size distribution does not vary.
- Icy particles are released from the fragmentation of fluffy dust particles in the coma. Their low abundance indicates that the latter are dehydrated upon arrival at Rosetta.
- Two kinds of outburst were observed; one is «dusty» (and richer in water) and the other one is «gaseous» (richer in CO₂).
- A new model of comet formation and activity was developed. The comet nucleus includes meter-sized blocks rich in water ice (WEBs), which are progressively exposed by CO₂ activity while approaching the sun, leading to surface's bluing and triggering water ice activity. These blocks are eventually eroded by water-driven dust ejection and covered by the infall of dehydrated dust, decreasing the contribution of water activity when the comet is far from perihelion.
- Parameters describing the translational and rotational motion of dust particles in the coma were defined.

Author Contributions: Conceptualization, project administration & writing—original draft preparation: A.L.; Methodology, investigation: all authors. All authors have read and agreed to the published version of the manuscript.

Funding: This work was supported by the International Space Science Institute (ISSI) through the ISSI International Team ‘Characterization of cometary activity of 67P/Churyumov–Gerasimenko comet’. Work by B.P. and M.R. was funded by the Canton of Bern and the Swiss National Science Foundation (200020_207312).

Data Availability Statement: The ESA’s Rosetta Planetary Science Archive is available at <https://archives.esac.esa.int/psa/#!Table%20View/Rosetta=mission> (accessed on 10 October 2023).

Conflicts of Interest: The authors declare no conflict of interest.

References

1. Coradini, A.; Capaccioni, F.; Drossart, P.; Arnold, G.; Ammannito, E.; Angrilli, F.; Barucci, A.; Bellucci, G.; Benkhoff, J.; Bianchini, G.; et al. Virtis: An Imaging Spectrometer for the Rosetta Mission. *Space Sci. Rev.* **2007**, *128*, 529–559. [\[CrossRef\]](#)
2. Longobardo, A.; Mannel, T.; Kim, M.; Fulle, M.; Rotundi, A.; Della Corte, V.; Rinaldi, G.; Lasue, J.; Merouane, S.; Cottin, H.; et al. Combining Rosetta’s GIADA and MIDAS data: Morphological versus dynamical properties of dust at 67P/Churyumov–Gerasimenko. *Mon. Not. R. Astron. Soc.* **2022**, *516*, 5611–5617. [\[CrossRef\]](#)
3. Longobardo, A.; Palomba, E.; Capaccioni, F.; Ciarniello, M.; Tosi, F.; Mottola, S.; Moroz, L.V.; Filacchione, G.; Raponi, A.; Quirico, E.; et al. Photometric behaviour of 67P/Churyumov–Gerasimenko and analysis of its pre-perihelion diurnal variations. *Mon. Not. R. Astron. Soc.* **2017**, *469*, S346–S356. [\[CrossRef\]](#)
4. Terada, H.; Tokunaga, A.T.; Kobayashi, N.; Takato, N.; Hayano, Y.; Takami, H. Detection of Water Ice in Edge-on Protoplanetary Disks: HK Tauri B and HV Tauri C. *Astrophys. J.* **2007**, *667*, 303–307. [\[CrossRef\]](#)
5. Berrezueta, E.; Cuervas-Mons, J.; Rodruguez-Rey, A.; Ordonez-Casado, B. Representativity of 2D Shape Parameters for Mineral Particles in Quantitative Petrography. *Minerals* **2019**, *9*, 768. [\[CrossRef\]](#)
6. Della Corte, V.; Rotundi, A.; Fulle, M.; Ivanovski, S.; Green, S.F.; Rietmeijer, F.J.M.; Colangeli, L.; Palumbo, P.; Sordini, R.; Ferrari, M.; et al. 67P/C-G inner coma dust properties from 2.2 au inbound to 2.0 au outbound to the Sun. *Mon. Not. R. Astron. Soc.* **2016**, *469*, S210–S219. [\[CrossRef\]](#)
7. Ciarniello, M.; Fulle, M.; Raponi, A.; Filacchione, G.; Capaccioni, F.; Rotundi, A.; Rinaldi, G.; Formisano, M.; Magni, G.; Tosi, F. et al. Macro and micro- structures of pebble-made cometary nuclei reconciled by seasonal evolution. *Nat. Astron.* **2022**, *6*, 546–553. [\[CrossRef\]](#)

8. Colangeli, L.; Lopez-Moreno, J.J.; Palumbo, P.; Rodriguez, J.; Cosi, M.; Della Corte, V.; Esposito, F.; Fulle, M.; Herranz, M.; Jeronimo, J.M.; et al. The Grain Impact Analyser and Dust Accumulator (GIADA) Experiment for the Rosetta Mission: Design, Performances and First Results. *Space Sci. Rev.* **2007**, *128*, 803–821. [\[CrossRef\]](#)
9. Riedler, W.; Torkar, K.; Jeszenszky, H.; Romstedt, J.; Alleyne, H.S.C.; Arends, H.; Barth, W.; Biezen, J.V.D.; Butler, B.; Ehrenfreud, P. MIDAS The Micro-Imaging Dust Analysis System for the Rosetta Mission. *Space Sci. Rev.* **2007**, *128*, 869–904. [\[CrossRef\]](#)
10. De Sanctis, M.C.; Capaccioni, F.; Ciarniello, M.; Filacchione, G.; Formisano, M.; Mottola, S.; Raponi, A.; Tosi, F.; Bockelee-Morvan, D.; Erard, S.; et al. The diurnal cycle of water ice on comet 67P/Churyumov-Gerasimenko. *Nature* **2015**, *525*, 500–503. [\[CrossRef\]](#)
11. Pestoni, B.; Altwegg, K.; Balsiger, H.; Hanni, N.; Rubin, M.; Schroeder, I.; Schuhmann, M.; Wampfler, S. Detection of volatiles undergoing sublimation from 67P/Churyumov-Gerasimenko coma particles using ROSINA/COPS. II. The nude gauge. *Astron. Astrophys.* **2021**, *651*, A26. [\[CrossRef\]](#)
12. Noonan, J.W.; Rinaldi, G.; Feldman, P.D.; Stern, S.A.; Parker, J.W.; Keeney, B.A.; Bockelee-Morvan, D.; Vervack, R.J., Jr.; Steffl, A.J.; Knight, M.M.; et al. Analysis of hybrid gas-dust outbursts observed at 67P/Churyumov-Gerasimenko. *Astron. J.* **2021**, *162*, 4.
13. Bentley, M.S.; Schmied, R.; Mannel, T.; Torkar, K.; Jeszenszky, H.; Romstedt, J.; Levasseur-Regourd, A.-C.; Weber, I.; Jessberger, E.K.; Ehrenfreud, P.; et al. Aggregate dust particles at comet 67P/Churyumov-Gerasimenko. *Nature* **2016**, *537*, 73–75. [\[CrossRef\]](#)
14. Lasue, J.; Maroger, I.; Botet, R.; Garnier, P.; Merouane, S.; Mannel, T.; Levasseur-Regourd, A.-C.; Bentley, M.S. Flattened loose particles from numerical simulations compared to particles collected by Rosetta. *Astron. Astrophys.* **2019**, *630*, A28. [\[CrossRef\]](#)
15. El-Maarry, M.R.; Thomas, N.; Giacomini, L.; Massironi, M.; Pajola, M.; Marschall, R.; Gracia-Bernà, A.; Sierks, H.; Barbieri, C.; Lamy, P.L.; et al. Regional surface morphology of comet 67P/Churyumov-Gerasimenko from Rosetta/OSIRIS images. *Astron. Astrophys.* **2015**, *583*, A26. [\[CrossRef\]](#)
16. El-Maarry, M.R.; Thomas, N.; Gracia-Bernà, A.; Pajola, M.; Lee, J.-C.; Massironi, M.; Davidsson, B.; Marchi, S.; Keller, H.U.; Hviid, S.F.; et al. Regional surface morphology of comet 67P/Churyumov-Gerasimenko from Rosetta/OSIRIS images: The southern hemisphere. *Astron. Astrophys.* **2016**, *593*, A110. [\[CrossRef\]](#)
17. Keller, H.U.; Barbieri, C.; Lamy, P.; Rickman, H.; Rodrigo, R.; Wenzel, K.-P.; Sierks, H.; A'Hearn, M.F.; Angrilli, F.; Angulo, M.; et al. OSIRIS The Scientific Camera System Onboard Rosetta. *Space Sci. Rev.* **2007**, *128*, 433–506. [\[CrossRef\]](#)
18. Rinaldi, G.; Bockelee-Morvan, D.; Ciarniello, M.; Tozzi, G.P.; Capaccioni, F.; Ivanovski, S.L.; Filacchione, G.; Fink, U.; Doose, L.; Taylor, F.; et al. Summer outbursts in the coma of comet 67P/Churyumov-Gerasimenko as observed by Rosetta-VIRTIS. *Mon. Not. R. Astron. Soc.* **2018**, *481*, 1235–1250. [\[CrossRef\]](#)
19. Hu, X.; Shi, X.; Sierks, H.; Fulle, M.; Blum, J.; Keller, H.U.; Kuhrt, E.; Davidsson, B.; Guttler, C.; Gundlach, B.; et al. Seasonal erosion and restoration of the dust cover on comet 67P/Churyumov-Gerasimenko as observed by OSIRIS onboard Rosetta. *Astron. Astrophys.* **2017**, *604*, A114. [\[CrossRef\]](#)
20. Combi, M.; Shou, Y.; Fougere, N.; Tenishev, V.; Altwegg, K.; Rubin, M.; Bockelee-Morvan, D.; Capaccioni, F.; Cheng, Y.-C.; Fink, U.; et al. The surface distributions of the production of the major volatile species, H₂O, CO₂, CO and O₂, from the nucleus of comet 67P/Churyumov-Gerasimenko throughout the Rosetta Mission as measured by the ROSINA double focusing mass spectrometer. *Icarus* **2019**, *335*, 113421. [\[CrossRef\]](#)
21. Ellerbroek, L.E.; Gundlach, B.; Landeck, A.; Dominik, C.; Blum, J.; Merouane, S.; Hilchenbach, M.; Bentley, M.S.; Mannel, T.; John, H.; et al. The footprint of cometary dust analogues—I. Laboratory experiments of low-velocity impacts and comparison with Rosetta data. *Mon. Not. R. Astron. Soc.* **2017**, *469*, S204–S206. [\[CrossRef\]](#)
22. Balsiger, H.; Altwegg, K.; Bochsler, P.; Eberhardt, P.; Fischer, J.; Graf, S.; Jackel, A.; Kopp, E.; Langer, U.; Mildner, M.; et al. Rosina Rosetta Orbiter Spectrometer for Ion and Neutral Analysis. *Space Sci. Rev.* **2007**, *128*, 745–801. [\[CrossRef\]](#)
23. Stern, S.A.; Slater, D.C.; Scherrer, J.; Stone, J.; Versteeg, M.; A'Hearn, M.F.; Bertaux, J.L.; Feldman, P.D.; Festou, M.C.; Parker, J.W.; et al. Alice: The Rosetta Ultraviolet Imaging Spectrograph. *Space Sci. Rev.* **2007**, *128*, 507–527. [\[CrossRef\]](#)
24. Longobardo, A.; Della Corte, V.; Ivanovski, S.; Rinaldi, G.; Zakharov, V.; Rotundi, A.; Capaccioni, F.; Fulle, M.; Filacchione, G.; Palomba, E.; et al. 67P/Churyumov-Gerasimenko active areas before perihelion identified by GIADA and VIRTIS data fusion. *Mon. Not. R. Astron. Soc.* **2019**, *483*, 2165–2176. [\[CrossRef\]](#)
25. Longobardo, A.; Della Corte, V.; Rotundi, A.; Fulle, M.; Rinaldi, G.; Formisano, M.; Zakharov, V.; Ivanovski, S.; Mannel, T.; Ciarniello, M.; et al. 67P/Churyumov-Gerasimenko's dust activity from pre- to post-perihelion as detected by Rosetta/GIADA. *Mon. Not. R. Astron. Soc.* **2020**, *496*, 125–137. [\[CrossRef\]](#)
26. Capaccioni, F.; Coradini, A.; Filacchione, G.; Erard, S.; Arnold, G.; Drossart, P.; De Sanctis, M.C.; Bockelee-Morvan, D.; Capria, M.T.; Tosi, F.; et al. The organic-rich surface of comet 67P/Churyumov-Gerasimenko as seen by VIRTIS/Rosetta. *Science* **2015**, *347*, aaa0628. [\[CrossRef\]](#) [\[PubMed\]](#)
27. Schulz, R.; Hilchenbach, M.; Langevin, Y.; Kissel, J.; Silen, J.; Brois, C.; Engrand, C.; Hornung, K.; Baklouti, D.; Bardyn, A.; et al. Comet 67P/Churyumov-Gerasimenko sheds dust coat accumulated over the past four years. *Nature* **2015**, *518*, 216–218. [\[CrossRef\]](#)
28. Zakharov, V.V.; Rotundi, A.; Della Corte, V.; Fulle, M.; Ivanovski, S.L.; Rodionov, A.V.; Bykov, N.Y. On the similarity of dust flows in the inner coma of comets. *Icarus* **2021**, *364*, 114476. [\[CrossRef\]](#)
29. Mannel, T.; Bentley, M.S.; Schmied, R.; Jeszenszky, H.; Levasseur-Regourd, A.C.; Romstedt, J.; Torkar, K. Fractal cometary dust—A window into the early Solar system. *Mon. Not. R. Astron. Soc.* **2016**, *462*, S304–S311. [\[CrossRef\]](#)
30. Paquette, J.A.; Engrand, C.; Stenzel, O.; Hilchenbach, M.; Kissel, J. Searching for calcium-aluminum-rich inclusions in cometary particles with Rosetta/COSIMA. *Meteoritics Planet. Sci.* **2016**, *51*, 1340–1352. [\[CrossRef\]](#)

31. Ciarletti, V.; Herique, A.; Lasue, J.; Levasseur-Regourd, A.-C.; Plettemeir, D.; Lemmonier, F.; Guiffaut, C.; Pasquero, P.; Kofman, W. CONSERT constrains the internal structure of 67P at a few metres size scale. *Mon. Not. R. Astron. Soc.* **2017**, *469*, S805–S817. [\[CrossRef\]](#)
32. Kramer, T.; Lauter, M.; Rubin, M.; Altwegg, K. Seasonal changes of the volatile density in the coma and on the surface of comet 67P/Churyumov-Gerasimenko. *Mon. Not. R. Astron. Soc.* **2017**, *469*, S20–S28. [\[CrossRef\]](#)
33. Ciarniello, M.; Raponi, A.; Capaccioni, F.; Filacchione, G.; Tosi, F.; De Sanctis, M.C.; Kappel, D.; Rousseau, B.; Arnold, G.; Capria, M.T.; et al. The global surface composition of 67P/Churyumov-Gerasimenko nucleus by Rosetta/VIRTIS. II) Diurnal and seasonal variability. *Mon. Not. R. Astron. Soc.* **2016**, *462*, S443–S458. [\[CrossRef\]](#)
34. L  uter, M.; Kramer, T.; Rubin, M.; Altwegg, K. Gas production of comet 67P/Churyumov-Gerasimenko reconstructed from DFMS/COPS data. *EPSC Abstr.* **2018**, *12*, EPSC2018-515-1.
35. Raponi, A.; Ciarniello, M.; Capaccioni, F.; Mennella, V.; Filacchione, G.; Vinogradoff, V.; Poch, O.; Beck, P.; Quirico, E.; De Sanctis, M.C.; et al. Infrared detection of aliphatic organics on a cometary nucleus. *Nat. Astron.* **2020**, *4*, 500–505. [\[CrossRef\]](#)
36. Pestoni, B.; Altwegg, K.; Della Corte, V.; Hanni, N.; Longobardo, A.; Muller, D.R.; Rotundi, A.; Rubin, M.; Wampl  er, S.F. Multi-instrument analysis of 67P/Churyumov-Gerasimenko coma particles: COPS-GIADA data fusion. *Astron. Astrophys.* **2023**, *671*, A168. [\[CrossRef\]](#)
37. Pajola, M.; Lucchetti, A.; Fulle, M.; Mottola, S.; Hamm, M.; Da Deppo, V.; Penasa, L.; Kovacs, G.; Massironi, M.; Shi, X.; et al. The pebbles/boulders size distributions on Sais: Rosetta’s final landing site on comet 67P/Churyumov-Gerasimenko. *Mon. Not. R. Astron. Soc.* **2017**, *469*, S636–S645. [\[CrossRef\]](#)
38. Bockelee-Morvan, D.; Rinaldi, G.; Erard, S.; Leyrat, C.; Capaccioni, F.; Drossart, P.; Filacchione, G.; Migliorini, A.; Quirico, E.; Mottola, S.; et al. Comet 67P outbursts and quiescent coma at 1.3 au from the Sun: Dust properties from Rosetta/VIRTIS-H observations. *Mon. Not. R. Astron. Soc.* **2017**, *469*, S443–S458. [\[CrossRef\]](#)
39. Mannel, T.; Bentley, M.S.; Boakes, P.D.; Jeszenszky, H.; Ehrenfreund, P.; Engrand, C.; Koeberl, C.; Levasseur-Regourd, A.C.; Romstedt, J.; Schmied, R.; et al. Dust of comet 67P/Churyumov-Gerasimenko collected by Rosetta/MIDAS: Classification and extension to the nanometer scale. *Astron. Astrophys.* **2019**, *630*, A26. [\[CrossRef\]](#)
40. Rinaldi, G.; Fink, U.; Doose, L.; Tozzi, G.P.; Capaccioni, F.; Filacchione, G.; Bockelee-Morvan, D.; Leyrat, C.; Piccioni, G.; Erard, S.; et al. Properties of the dust in the coma of 67P/Churyumov-Gerasimenko observed with VIRTIS-M. *Mon. Not. R. Astron. Soc.* **2016**, *462*, S547–S561. [\[CrossRef\]](#)
41. Feldman, P.D.; A’Hearn, M.F.; Feaga, L.M.; Bertaux, J.-L.; Noonan, J.; Parker, J.W.; Schindhelm, R.; Steffl, A.J.; Stern, S.A.; Weaver, H.A. The nature and frequency of the gas outbursts in comet 67P/Chryumov-Gerasimenko observed by the Alice far-ultraviolet spectrograph on Rosetta. *Astrophys. J. Lett.* **2016**, *825*, L8. [\[CrossRef\]](#)
42. Fray, N.; Bardyn, A.; Cottin, H.; Altwegg, K.; Baklouti, D.; Briois, C.; Colangeli, L.; Engrand, C.; Fischer, H.; Glasmachers, A.; et al. High-molecular-weight organic matter in the particles of comet 67P/Churyumov-Gerasimenko. *Nature* **2016**, *538*, 72–74. [\[CrossRef\]](#) [\[PubMed\]](#)
43. Fornasier, S.; Hoang, H.V.; Fulle, M.; Quirico, E.; Ciarniello, M. Volatile exposures on the 67P/Churyumov-Gerasimenko nucleus. *Astron. Astrophys.* **2023**, *672*, A136. [\[CrossRef\]](#)
44. Ivanovski, S.L.; Zakharov, V.V.; Moreno, F.; Bykov, N.Y.; Munoz, O.; Fulle, M.; Rotundi, A.; Della Corte, V.; Rodionov, A.V. On the similarity of rotational motion of dust grains in the inner atmosphere of comets. *Mon. Not. R. Astron. Soc.* **2023**, in press. [\[CrossRef\]](#)
45. Kissel, J.; Altwegg, K.; Clark, B.C.; Colangeli, L.; Cottin, H.; Czempiel, S.; Eibl, J.; Engrand, C.; Fehring  er, H.M.; Feuerbacher, B.; et al. Cosima High Resolution Time-of-Flight Secondary Ion Mass Spectrometer for the Analysis of Cometary Dust Particles onboard Rosetta. *Space Sci. Rev.* **2007**, *128*, 823–867. [\[CrossRef\]](#)
46. Merouane, S.; Zaprudin, B.; Stenzel, O.; Langevin, Y.; Altobelli, N.; Della Corte, V.; Fischer, H.; Fulle, M.; Hornung, K.; Silen, J.; et al. Dust particle flux and size distribution in the coma of 67P/Churyumov-Gerasimenko measured in situ by the COSIMA instrument on board Rosetta. *Astron. Astrophys.* **2016**, *596*, A87. [\[CrossRef\]](#)
47. Poch, O.; Istiqomah, I.; Quirico, E.; Beck, P.; Schmitt, B.; Theul  , P.; Faure, A.; Hily-Blant, P.; Bonal, L.; Raponi, A.; et al. Ammonium salts are a reservoir of nitrogen on a cometary nucleus and possibly on some asteroids. *Science* **2020**, *367*, aaw7462. [\[CrossRef\]](#)
48. Moreno, F.; Guirado, D.; Munoz, O.; Zakharov, V.; Ivanovski, S.L.; Fulle, M.; Rotundi, A.; Frattin, E.; Bertini, I. Dynamics of irregularly shaped cometary particles subjected to outflowing gas and solar radiative forces and torques. *Mon. Not. R. Astron. Soc.* **2022**, *510*, 5142–5253. [\[CrossRef\]](#)
49. Altwegg, K.; Balsiger, H.; Berthel  ier, J.J.; Bieler, A.; Calmonte, U.; Fuselier, S.A.; Goesmann, F.; Gasc, S.; Gombosi, T.I.; Le Roy, L.; et al. Organics in comet 67P—A first comparative analysis of mass spectra from ROSINA-DFMS, COSAC and Ptolemy. *Mon. Not. R. Astron. Soc.* **2017**, *469*, S130–S141. [\[CrossRef\]](#)
50. Kim, M. et al. [Midas Team] Cometary dust collected by MIDAS on board Rosetta. I. Dust particle catalog and statistics. *Astron. Astrophys.* **2023**, *673*, A129. [\[CrossRef\]](#)
51. Kim, M. et al. [Rosina Team] Evolution of water production of 67P/Churyumov-Gerasimenko: An empirical model and a multi-instrument study. *Mon. Not. R. Astron. Soc.* **2016**, *462*, S491–S506.
52. Kim, M. et al. [MIDAS Team] Cometary dust collected by MIDAS on board Rosetta. II. Particle shape descriptors and pristinity evaluation. *Astron. Astrophys.* **2023**, in press.

53. Filacchione, G.; De Sanctis, M.C.; Capaccioni, F.; Raponi, A.; Tosi, F.; Ciarniello, M.; Cerroni, P.; Piccioni, G.; Capria, M.T.; Palomba, E.; et al. Exposed water ice on the nucleus of comet 67P/Churyumov-Gerasimenko. *Nature* **2016**, *529*, 368–372. [[CrossRef](#)] [[PubMed](#)]
54. Filacchione, G.; Capaccioni, F.; Ciarniello, M.; Raponi, A.; Tosi, F.; De Sanctis, M.C.; Erard, S.; Bockelee-Morvan, D.; Leyrat, C.; Arnold, G.; et al. The global surface composition of 67P/CG nucleus by Rosetta/VIRTIS. (I) Prelanding mission phase. *Icarus* **2016**, *274*, 334–349. [[CrossRef](#)]
55. Ivanovski, S.L.; Della Corte, V.; Rotundi, A.; Fulle, M.; Fougere, N.; Bieler, A.; Rubin, M.; Ivanovska, S.; Liuzzi, V. Dynamics of non-spherical dust in the coma of 67P/Churyumov-Gerasimenko constrained by GIADA and ROSINA data. *Mon. Not. R. Astron. Soc.* **2017**, *469*, S774–S786. [[CrossRef](#)]
56. Zakharov, V.V.; Ivanovski, S.L.; Crifo, J.-F.; Della Corte, V.; Rotundi, A.; Fulle, M. Asymptotics for spherical particle motion in a spherically expanding flow. *Icarus* **2018**, *312*, 121–127. [[CrossRef](#)]
57. Fulle, M.; Blum, J.; Rotundi, A.; Gundlach, B.; Guttler, C.; Zakharov, V. How comets work: Nucleus erosion versus dehydration. *Mon. Not. R. Astron. Soc.* **2020**, *469*, 4039–4044. [[CrossRef](#)]
58. Langevin, Y.; Hilchenbach, M.; Ligier, N.; Merouane, S.; Hornung, K.; Engrand, C.; Schulz, R.; Kissel, J.; Ryno, J.; Eng, P. Typology of dust particles collected by the COSIMA mass spectrometer in the inner coma of 67P/Churyumov Gerasimenko. *Icarus* **2016**, *271*, 76–97. [[CrossRef](#)]
59. Rinaldi, G.; Noonan, J.W.; Bockelée-Morvan, D.; Longobardo, A.; Migliorini, A.; Ciarniello, M.; Raponi, A.; Filacchione, G.; Capaccioni, F. Analysis of gas-dust outbursts observed at 67P/Churyumov-Gerasimenko. In Proceedings of the 16th Europlanet Science Congress 2022, Granada, Spain, 18–23 September 2022; EPSC2022-509.
60. Blum, J.; Gundlach, B.; Krause, M.; Fulle, M.; Johansen, A.; Agarwal, J.; van Bostel, I.; Shi, X.; Hu, X.; Bentley, M.S.; et al. Evidence for the formation of comet 67P/Churyumov-Gerasimenko through gravitational collapse of a bound clump of pebbles. *Mon. Not. R. Astron. Soc.* **2017**, *469*, S755–S773. [[CrossRef](#)]
61. Patzold, M.; Andert, T.P.; Hahn, M.; Barriot, J.-P.; Asmar, S.W.; Hausler, B.; Bird, M.K.; Tellmann, S.; Oschlisniok, J.; Peter, K. The Nucleus of comet 67P/Churyumov-Gerasimenko—Part I: The global view—nucleus mass, mass-loss, porosity, and implications. *Mon. Not. R. Astron. Soc.* **2019**, *483*, 2337–2346. [[CrossRef](#)]
62. Tubiana, C.; Snodgrass, C.; Bertini, I.; Mottola, S.; Vincent, J.-B.; Lara, L.; Fornasier, S.; Knollenberg, J.; Thomas, N.; Fulle, M.; et al. 67P/Churyumov-Gerasimenko: Activity between March and June 2014 as observed from Rosetta/OSIRIS. *Astron. Astrophys.* **2015**, *573*, A62. [[CrossRef](#)]
63. Pestoni, B.; Altwegg, K.; Balsiger, H.; Hanni, N.; Rubin, M.; Schroeder, I.; Schuhmann, M.; Wampfler, S. Detection of volatiles undergoing sublimation from 67P/Churyumov-Gerasimenko coma particles using ROSINA/COPS. I. The ram gauge. *Astron. Astrophys.* **2021**, *645*, A38. [[CrossRef](#)]
64. Filacchione, G.; Raponi, A.; Capaccioni, F.; Ciarniello, M.; Tosi, F.; Capria, M.T.; De Sanctis, M.C.; Migliorini, A.; Piccioni, G.; Cerroni, P.; et al. Seasonal exposure of carbon dioxide ice on the nucleus of comet 67P/Churyumov-Gerasimenko. *Science* **2016**, *354*, 1563–1566. [[CrossRef](#)] [[PubMed](#)]
65. Fulle, M.; Blum, J. Fractal dust constrains the collisional history of comets. *Mon. Not. R. Astron. Soc.* **2017**, *469*, S39–S44. [[CrossRef](#)]
66. Haser, L. Distribution d’intensité dans la tête d’une comète. *Bull. Cl. Sci. L’académie R. Belg.* **1957**, *43*, 740–750. [[CrossRef](#)]

Disclaimer/Publisher’s Note: The statements, opinions and data contained in all publications are solely those of the individual author(s) and contributor(s) and not of MDPI and/or the editor(s). MDPI and/or the editor(s) disclaim responsibility for any injury to people or property resulting from any ideas, methods, instructions or products referred to in the content.